

# Computational evaluation on reactivity, stability, and Hirshfeld surface analysis of caffeine-maleic acid cocrystal: Insights into molecular interactions

Tirth Raj Paneru<sup>a,b\*</sup>, Basanti Bhandari<sup>c</sup>

<sup>a</sup>Central Department of General Science, Far Western University, Kanchanpur, 10400, Nepal

<sup>b</sup>Central Department of Physics, Tribhuvan University, Kirtipur, Kathmandu, Nepal

<sup>c</sup>Bajjnath Secondary School Mahendranagar Kanchanpur, Nepal

## Research Article

©RMC (SNSC), Tribhuvan University

ISSN: 3059-9504 (online)

This work is licensed under the Creative

Commons CC BY-NC License.

<https://creativecommons.org/licenses/by-nc/4.0/>

## Article History

Received: November 2, 2024

Revised: November 18, 2024

Accepted: November 20, 2024

Published: December 28, 2024

## Keywords

Caffeine-maleic acid, Cocrystal, Hirshfeld surface, Molecular electrostatic potential, QTAIM

## \*Corresponding author

Email: [tirthpaneru2015@gmail.com](mailto:tirthpaneru2015@gmail.com) (T.R. Paneru)

Phone: +977-9845397970

## ABSTRACT

This work presents a computational evaluation of the caffeine-maleic acid cocrystal using density functional theory at the B3LYP/6-311++G(d,p) level of theory to gain a comprehensive understanding of molecular interaction. The purpose of this study is to use quantum chemical calculations to assess the strength of intra- and intermolecular interactions between API caffeine and coformer maleic acid, as well as within cocrystal, to predict the superiority of chemical reactivity and stability over API caffeine. The cocrystal was optimized, and geometrical parameters were compared to those parameters of crystal structure, which showed good agreement except at the intermolecular hydrogen bonding sites. The QTAIM analysis indicated a strong intermolecular hydrogen bond H29...N8 between caffeine and maleic acid, with strength of  $-16.152$  kcal/mol. This finding was also supported by the isosurface of the RDG scatter plot. The intermolecular hydrogen bonding interaction O...H was discovered to be significant in crystal packing, as evidenced by its 42.4% contribution to the Hirshfeld surface of the caffeine-maleic acid cocrystal. The electrostatic potential on the molecular surface of the cocrystal justified the sites H24 and O27 being proper for the nucleophilic and electrophilic attack with global maximum and minimum potential, which also support O...H intermolecular hydrogen bonding in the crystal packing of the caffeine-maleic acid cocrystal. The frontier molecular orbital energy gap in the caffeine-maleic acid cocrystal was found to be 4.018 eV, which is less than the energy gap in API caffeine, implying that the cocrystal is more reactive, polarizable, and kinetically less stable than caffeine.

## 1. INTRODUCTION

Cocrystals are a new type of crystalline material held together by non-ionic and non-covalent interactions and consist of two or more different molecules in a single crystal lattice in a specific ratio [1]. "Pharmaceutical cocrystals consist of at least one active pharmaceutical ingredient (API) and another non-toxic coformer that meets pharmaceutical approval" [2]. The use of pharmaceutical cocrystals in drug discovery is increasingly popular as it can enhance the stability, reactivity, bioavailability, solubility, dissolution profiles, and therapeutic effects of the drug [3]. Carboxylic acid functional groups are widely used as cofomers during the formation of cocrystals in drug design discovery [4]. Conventional hydrogen bonds, including N-H...O, N-H...N, O-H...O, and O-H...N interactions, are responsible for the majority of pharmaceutical cocrystal formation [5]. Caffeine is a naturally occurring drug that stimulates the central nervous system and belongs to the methylxanthine class [6]. Caffeine is most commonly found in coffee, tea, cacao beans, dairy products, energy drinks, and chocolate [7]. Caffeine increases mental alertness, speeds up thought processes, reduces fatigue, delays sleep, and also alleviates headaches and pain [8]. Caffeine is unstable in humid environments and forms non-stoichiometric hydrates. Dicarboxylic acids were used as a cocrystal coformer to increase the stability of caffeine in the presence of humidity [9]. According to Trask *et al.*, the caffeine-maleic acid cocrystal in 2:1 and 1:1 stoichiometric measurements made using solution precipitation and solid-state grinding exhibits stability concerning humidity. The binary and ternary phase diagrams of caffeine-maleic acid cocrystals in 1:1 and 2:1 ratios in solvent acetone can be used to validate stability [10]. Leyssens *et al.*, investigated the crystallization of caffeine-maleic acid in the

solvent under suitable conditions through nucleation growth, resulting in the formation of a cocrystal that improved its physicochemical characteristics [11]. The study conducted by Aher *et al.* found that the molar ratio of the caffeine-maleic acid cocrystal component in solution is a crucial parameter for large solubility differences [12].

The literature reveals that researchers have reported the crystallographic structure and other experimental studies to enhance the physicochemical properties of caffeine-maleic cocrystals. The caffeine-maleic acid cocrystal is still of interest for a DFT study. Our study intends to investigate the superiority of the caffeine-maleic acid cocrystal over the active pharmaceutical ingredient (API) as caffeine and the coformer as maleic acid by performing a computational evaluation using density functional theory (DFT). This study provides insight into the intra- and intermolecular hydrogen bonding, reactive sites, reactivity, and stability of the caffeine cocrystal with maleic acid. Density functional theory is used to calculate the quantum chemical using the hybrid functional B3LYP in the basis set 6-311++G(d,p). QTAIM analysis is used to analyze the electronic structure of cocrystals using the topology of electron density. The non-covalent interactions in the molecules are visualized via RDG scatter plot. Hirshfeld surface analysis allows for the quantification of the percentage of different interactions in the molecule. The electrostatic potential surface provides a key understanding of the reactive sites of the molecule. The natural bond orbital (NBO) analysis provides a clear understanding of bonding and interactions. The energy gap between the highest occupied and lowest unoccupied molecular orbitals was used to estimate the reactivity and stability of cocrystals over API caffeine.

## 2. MATERIALS AND METHODOLOGY

### 2.1 Computational details

The geometry optimization of the molecular structure has been done using density functional theory in the Gaussian 09 software package [13,14]. The basis set 6-311++G(d,p), which incorporates both polarization diffusion functions, was used with the hybrid functional B3LYP [15,16]. The optimized molecular structure and molecular orbitals, such as HOMO and LUMO, of the cocrystal were visualized using GaussView 05 [17]. The AIMALL software package was used to create a molecular graph depicting intra- and intermolecular interactions in the cocrystal [18]. Crystal Explorer software was used to conduct Hirshfeld surface analysis and plot fingerprints of interaction in the cocrystal [19]. The RDG plot and its isosurface in support of non-covalent interactions and electrostatic potential on the molecular surface were rendered from Multiwfn 8.0 and VMD 1.9.4 software [20,21]. The total density of state (DOS) was performed with GaussSum 3.0 software [22]. The natural bond orbital (NBO) analysis was employed for the evaluation of hyperconjugative charge transfer interactions by using the NBO 3.0 program included in the Gaussian 09 software [23].

## 3. RESULTS AND DISCUSSION

### 3.1 Geometry optimization

The crystal structure of the caffeine-maleic acid cocrystal (CCDC 272622) was obtained from the crystal structure database and optimized by using DFT in Gaussian software 09 with B3LYP/6-311++G(d,p) level of theory [24]. The optimized structure of the

caffeine-maleic acid cocrystal is shown in Fig. 1. The nitrogen of the caffeine ring and the carboxylic group of maleic acid form an intermolecular hydrogen bond O–H...N to form the cocrystal of caffeine. The ground state energy of caffeine cocrystal was found to be  $-713143.319$  kcal/mol. In contrast, the ground state energy of caffeine and maleic acid at the same level of theory were computed to be  $-427060.184$  and  $-286067.634$  kcal/mol, respectively. The interaction energy of the hydrogen bond was calculated by subtracting the energy sum of the cocrystal's constituents from its own energy, and it was found to be  $-15.501$  kcal/mol. The calculated optimized structural parameters (bond lengths and bond angles) of the caffeine-maleic acid cocrystal, along with the corresponding parameters of the crystal structure, are presented in Table 1. The bond lengths C11-H12, C11-H13, C11-H14, C15-H16, C15-H17, C15-H18, C19-H20, C19-H21, C19-H22, C23-H24, C32-H33, and C34-H35 differ from the experimental value by 0.111, 0.110, 0.106, 0.111, 0.111, 0.107, 0.109, 0.109, 0.109, 0.129, 0.135, and 0.135 Å, respectively. The bond angles C1-C10-O3, N2-C19-H20, C4-N9-C11, N5-C15-H18, N9-C11-H14, H26-O25-C31, H29-O28-C36, C31-C32-H33, H33-C32-C34, and C32-C34-H35 differ from experimental values by 1.2, 1.2, 2.4, 1.9, 2.0, 1.7, 4.2, 4.2, 2.9, and 2.5°, respectively. The main reason behind the variation of calculated data from the experimental value is that our calculation was performed in a gaseous medium. The intermolecular hydrogen bonding was not considered in gaseous medium, which plays a significant role in crystal packing.

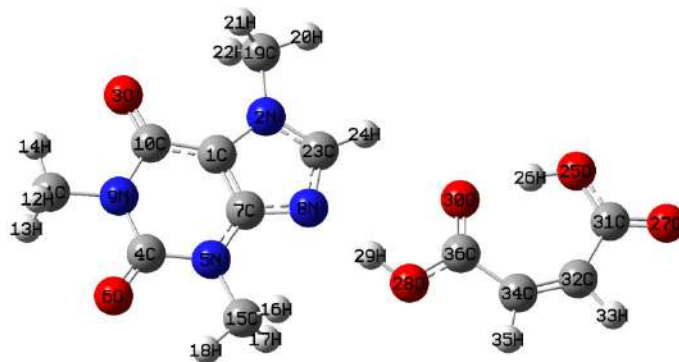


**Fig. 1:** The optimized structure of the caffeine-maleic acid cocrystal with numbering scheme.

**Table 1.** The optimized structure parameters (bond lengths and bond angles) of the caffeine-maleic acid cocrystal calculated at B3LYP/6-311++G(d,p) level of theory with the corresponding value of the experimental structure.

Bond Name	Bond length (Å)	Experimental <sup>a</sup>	Angle Name	Angle (°)	Experimental <sup>a</sup>
R(C1-N2)	1.388	1.390	A(N2-C1-C7)	105.5	105.7
R(C1-C7)	1.377	1.362	A(N2-C1-C10)	131.2	131.5
R(C1-C10)	1.434	1.424	A(C1-N2-C19)	126.8	127.0
R(N2-C19)	1.462	1.469	A(C1-N2-C23)	106.4	106.6
R(N2-C23)	1.345	1.327	A(C7-C1-C10)	123.2	122.7
R(O3-C10)	1.221	1.222	A(C1-C7-N5)	122.3	122.5
R(C4-N5)	1.398	1.380	A(C1-C7-N8)	110.7	110.6
R(C4-O6)	1.216	1.221	A(C1-C10-O3)	126.1	127.3
R(C4-N9)	1.407	1.399	A(C1-C10-N9)	111.2	111.6
R(N5-C7)	1.370	1.371	A(C19-N2-C23)	126.8	126.4

R(N5-C15)	1.465	1.473	A(N2-C19-H20)	108.3	109.5
R(C7-N8)	1.362	1.359	A(N2-C19-H21)	110.0	109.5
R(N8-C23)	1.336	1.342	A(N2-C19-H22)	110.0	109.5
R(N9-C10)	1.417	1.405	A(N2-C23-N8)	112.7	112.3
R(N9-C11)	1.470	1.470	A(N2-C23-H24)	123.8	123.8
R(C11-H12)	1.090	0.979	A(O3-C10-9)	122.6	121.1
R(C11-H13)	1.090	0.980	A(N5-C4-O6)	122.1	121.5
R(C11-H14)	1.086	0.980	A(N5-C4-N9)	116.9	116.8
R(C15-H16)	1.091	0.980	A(C4-N5-C7)	119.4	119.3
R(C15-H17)	1.091	0.980	A(C4-N5-C15)	119.8	119.9
R(C15-H18)	1.086	0.979	A(O6-C4-N9)	121.1	121.7
R(C19-H20)	1.089	0.980	A(C4-N9-C10)	127.0	127.0
R(C19-H21)	1.089	0.980	A(C4-N9-C11)	115.1	117.5
R(C19-H22)	1.089	0.980	A(C7-N5-C15)	120.9	120.9
R(C23-H24)	1.079	0.950	A(N5-C7-N8)	127.0	126.9
R(O25-H26)	0.991	0.987	A(N5-C15-H16)	110.1	109.5
R(O25-C31)	1.330	1.323	A(N5-C15-H17)	110.1	109.5
R(O27-C31)	1.209	1.212	A(N5-C15-H18)	107.6	109.5
R(O28-H29)	1.016	1.055	A(C7-N8-C23)	104.7	104.8
R(O28-C36)	1.317	1.286	A(N8-C23-H24)	123.5	123.9
R(O30-C36)	1.231	1.241	A(C10-N9-C11)	117.9	115.5
R(C31-C32)	1.509	1.488	A(N9-C11-H12)	109.9	109.4
R(C32-H33)	1.085	0.950	A(N9-C11-H13)	109.9	109.5
R(C32-C34)	1.343	1.329	A(N9-C11-H14)	107.5	109.5
R(C34-H35)	1.084	0.950	A(H12-C11-H13)	108.6	109.5
R(C34-C36)	1.483	1.485	A(H12-C11-H14)	110.5	109.5
R(N8-H29)	1.676	1.497	A(H13-C11-H14)	110.5	109.5
R(H26-O30)	1.626	1.529	A(H16-C15-H17)	109.2	109.5
			A(H16-C15-H18)	109.8	109.4
			A(H17-C15-H18)	109.8	109.5
			A(H20-C19-H21)	109.9	109.4
			A(H20-C19-H22)	109.9	109.5
			A(H21-C19-H22)	108.7	109.5
			A(H26-O25-C31)	111.6	109.9
			A(O25-C31-O27)	121.9	120.4
			A(O25-C31-C32)	120.2	120.0
			A(O27-C31-C32)	117.9	119.5
			A(H29-O28-C36)	110.8	115.0
			A(O28-C36-O30)	122.8	123.3
			A(O28-C36-C34)	112.1	113.4
			A(O30-C36-C34)	125.1	123.2
			A(C31-C32-H33)	109.6	113.8
			A(C31-C32-C34)	133.7	132.4
			A(H33-C32-C34)	116.7	113.8
			A(C32-C34-H35)	117.7	115.2
			A(C32-C34-C36)	128.9	129.5
			A(H35-C34-C36)	113.4	115.3

A(C7-N8-H29)	137.8	131.7
A(C23-N8-H29)	117.5	123.5
A(O25-H26-O30)	170.1	174.9
A(O28-H29-N8)	178.4	175.5
A(C36-O30-H26)	110.4	109.6

<sup>a</sup>Ref. [24]

### 3.2 QTAIM analysis

The quantum theory of atoms in molecules (QTAIM) is an analytical framework for understanding chemical bonds. It employs electron density to determine bond paths and their corresponding bond critical points [25]. The characteristics of the bond critical point (BCP) are analyzed from the electron density ( $\rho_{\text{BCP}}$ ), Laplacian of electron density ( $\nabla^2\rho_{\text{BCP}}$ ), and total electron density ( $H_{\text{BCP}}$ ), the sum of kinetic electron energy density ( $G_{\text{BCP}}$ ) and potential electron energy density ( $V_{\text{BCP}}$ ) [26]. The interaction energy in the formation of intermolecular hydrogen bonds can also be evaluated by taking half of the potential electron energy density. The electron density from

the calculation was found within the range (0.002–0.040) a.u., while the Laplacian electron density ranges (0.024–0.139) a.u., indicating that the bond critical point for the proton acceptor confirms the presence of the hydrogen bond [27]. The presence of a medium hydrogen bond that is partially covalent in nature was predicted by the Laplacian  $\nabla^2\rho_{\text{BCP}} > 0$  and  $H_{\text{BCP}} < 0$  values [28]. The molecular graph of the caffeine-maleic acid cocrystal with the visualization of hydrogen bond interactions is shown in Fig. 2. The topological parameters for the intra-molecular hydrogen bonds in the caffeine-maleic acid cocrystals and intermolecular hydrogen bond interactions between caffeine and maleic acid are presented in Table 2.

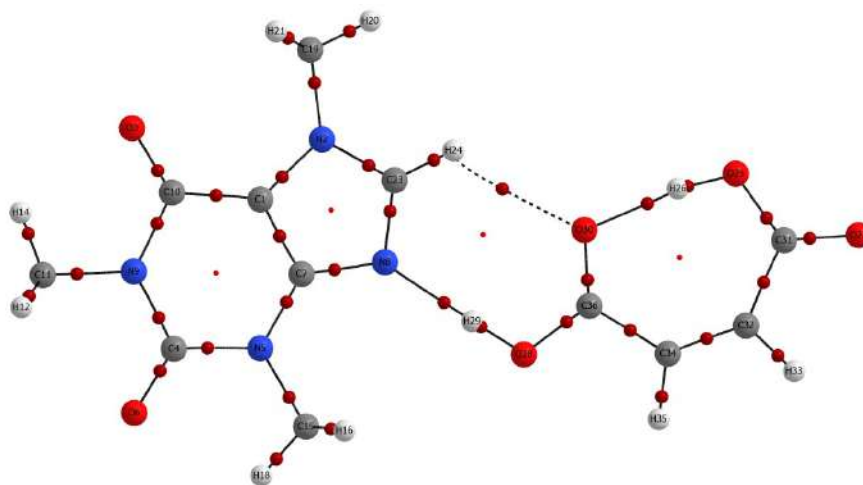


**Fig. 2:** The molecular graph showing intra- and intermolecular hydrogen bonding in the caffeine-maleic acid cocrystal.

**Table 2.** The topological parameters for the intra- and intermolecular hydrogen bonding in the caffeine-maleic acid cocrystal.

Interactions	Bond length (Å) (DFT)	Bond length (Å) in Crystal <sup>a</sup>	$\rho_{\text{BCP}}$	$G_{\text{BCP}}$	$V_{\text{BCP}}$	$\nabla^2\rho_{\text{BCP}}$	$H_{\text{BCP}}$	$E_{\text{int}}$	$\epsilon$
H29...N8	1.676	1.485	0.05579	0.01307	-0.05148	0.10133	-0.03841	-16.152	0.0469
H24...O30	2.465	2.708	0.00986	-0.00131	-0.00598	0.03443	-0.00729	-1.876	0.0746
H26...O30	1.626	1.529	0.05487	0.00865	-0.05568	0.15347	-0.04703	-17.470	0.0304

$\rho_{\text{BCP}}$ : Electron density at bond critical point (a.u),  $H_{\text{BCP}}$ : Total energy density (a.u),  $G_{\text{BCP}}$ : Kinetic energy density (a.u),  $E_{\text{int}}$ : Interaction energy (kcal/mol),  $V_{\text{BCP}}$ : Potential energy density (a.u),  $\nabla^2\rho_{\text{BCP}}$ : Laplacian of electron density (a.u),  $\epsilon$ : Bond ellipticity, <sup>a</sup>Ref. [24]

In the caffeine-maleic acid cocrystal, two intermolecular hydrogen bonds, H29...N8 and H24...O34, were observed. The H29...N8 bond has interaction energy of -16.152 kcal/mol, indicating a strong hydrogen bond. The total interaction energy for intermolecular interaction in the formation of the caffeine-maleic acid cocrystal from QTAIM calculations was found to be -18.128 kcal/mol, which was found to be comparable to the interaction energy of -15.501 kcal/mol found from the energy difference. The strong intra-molecular hydrogen bond H26...O30 exists, which has a interaction energy of -17.470 kcal/mol. The bond length of the intermolecular hydrogen bond H29...N8 between caffeine and maleic acid calculated from DFT was 1.676 Å, and its length in crystal structure was

1.485 Å. The bond angle of the hydrogen bond from DFT calculation was found to be 178.4°, and its corresponding value in crystal structure was 175.5°, showing good agreement.

### 3.3 Non-covalent interaction

Non-covalent interactions that do not involve the exchange of electron pairs between atoms include hydrogen bonds, van der Waals forces, and electrostatic interactions in molecular complexes based on electron density and its derivatives [29]. In our study, the non-covalent interactions were visualized and illustrated with the aid of the RDG scatter plot and its isosurface. The value of RDG is determined by the following relation [30]:

$$RDG(r) = \frac{1}{2(3\pi^2)^{\frac{1}{3}}} \frac{|\nabla\rho(r)|}{\rho(r)^{\frac{4}{3}}}$$

In the relation,  $\rho(r)$  is the electron density and  $\nabla\rho(r)$  represents the gradient of electron density. The graph plotted between the RDG value and  $\text{sign}\lambda_2(\rho)$  distinguishes different interactions, among them: green spikes stand for van der Waals interactions, red spikes for steric repulsion, and blue spikes represent hydrogen bond interactions [31]. The RDG scatter plot and its isosurface with the visualization of non-covalent interactions in caffeine-maleic acid cocrystals are shown in Fig. 3. (a) and (b) respectively. In the RDG scatter

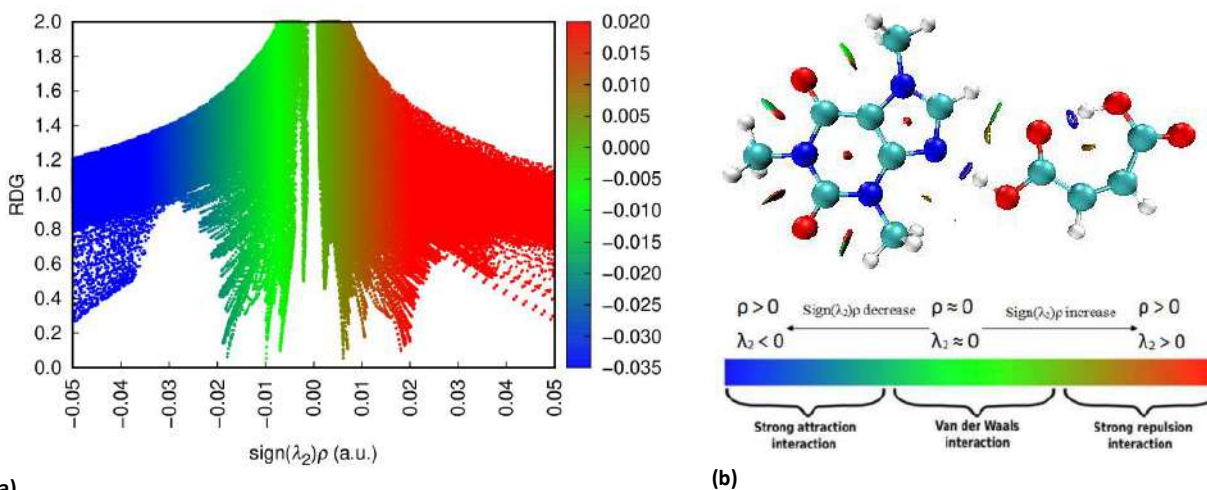


Fig. 3: (a) The RDG scatter plot and (b) isosurface showing non-covalent interactions in the caffeine-maleic acid cocrystal.

### 3.4 Hirshfeld surface analysis

The intermolecular interactions within a crystal structure can be quantitatively described and visualized through Hirshfeld surface analysis [32]. To analyze intermolecular interactions, we used the Hirshfeld surface mapped over  $d_{\text{norm}}$  and two-dimensional finger plots. The distance between the Hirshfeld surface and the interior atom is  $d_i$ , and the distance between the Hirshfeld surface and the exterior atom is  $d_e$ . The normalized distance  $d_{\text{norm}}$  measures the proximity of an atom from the Hirshfeld surface to another atom in the crystal structure when compared to the sum of their van der Waals radii, which is given by the relation [33].

$$d_{\text{norm}} = \frac{d_{i-r_i^{\text{vdw}}}}{r_i^{\text{vdw}}} + \frac{d_{e-r_e^{\text{vdw}}}}{r_e^{\text{vdw}}}$$

Where,  $r_i^{\text{vdw}}$  and  $r_e^{\text{vdw}}$  stands for the van der Waals radii. HS plotted mapped over  $d_{\text{norm}}$  and shape-index of crystal surface is shown in Fig. 4 (a) and (b), respectively. If  $d_{\text{norm}} < 0$ , then the distance between surface points and nearby atoms is shorter than the sum of van der Waals radii; hence, they make strong intermolecular interactions represented by the red spots for the H-bond donors and acceptors on the Hirshfeld surface. The blue regions of the Hirshfeld surface show  $d_{\text{norm}} > 0$ , and white regions have  $d_{\text{norm}} = 0$  [34]. Van der Waals interactions are indicated by the white regions of the Hirshfeld surface, while no interactions are observed in the blue regions. The red spot visualized in the HS of the molecule is for the strong intermolecular interaction C-H...O. The presence of red and blue triangles on the shape-indexed surface of the Hirshfeld surface indicates the presence of  $\pi$ - $\pi$  stacking in the cocrystal [35]. There are noticeable peaks in the region of nearly  $2.2 \text{ \AA} <$

graph, blue color spikes are observed between  $-0.03$  and  $-0.05$  a.u. This indicates a strong intermolecular hydrogen bond between N8 and H29, as well as an intra-molecular hydrogen bond between H26 and O30. These bonds are also seen in the molecular graph from the AIM study. The red color spikes, which are indicative of steric repulsion and are particularly noticeable in the caffeine ring, appear between  $0.02$  and  $0.05$  a.u. The hydrogen of the methyl moieties and the oxygen of the caffeine ring were found to be attracted to each other by a weak van der Waals force.

$d_e+d_i < 3.3 \text{ \AA}$  in the fingerprint plots shown in Fig. 5. The O...H interaction at  $d_e+d_i = 2.2 \text{ \AA}$  produced the most prominent long spikes, which provide the highest contribution of 42.4% to the total Hirshfeld surface. The wide and scattered large region of the finger plot covered by H...H interaction is due to the higher number of atoms, which contributed 31.8% to the Hirshfeld surface with tips at  $d_e+d_i = 2.4 \text{ \AA}$ . The C...C contact results from  $\pi$ - $\pi$  stacking, with triangle-shaped tips at  $d_e+d_i = 3.3 \text{ \AA}$ , contributing 5.5% to the Hirshfeld surface. The contributions from C...H and N...H interactions to the Hirshfeld surface are 5.9% and 4.1%, respectively. This indicates that O...H interactions play a significant role in crystal packing.

### 3.5 Electrostatic potential (ESP) surface analysis

The electrostatic potential on the molecular surface provides insight into intermolecular interactions in conjunction with molecular properties, including biological activity [36]. It aids in the prediction of electrophiles and nucleophiles by identifying the molecule's reactive sites. The most positive potential region of the molecular surface, highlighted in blue corresponds to electrophile, while the most negative potential region, highlighted in red belongs to a nucleophile. The electrostatic potential rises in the order of red, orange, yellow, green, and blue [37]. On the molecular electrostatic potential surface, the blue dot corresponds to the lowest potential and the orange dot to the highest potential [38]. The electrostatic potential surface for the caffeine-maleic acid cocrystal is shown in Fig. 6. The hydrogen atom in the methyl group is in the blue color region and has a positive electrostatic potential, which allows it to act as an electrophile. In contrast, the oxygen atoms of maleic acid and caffeine are in the red color

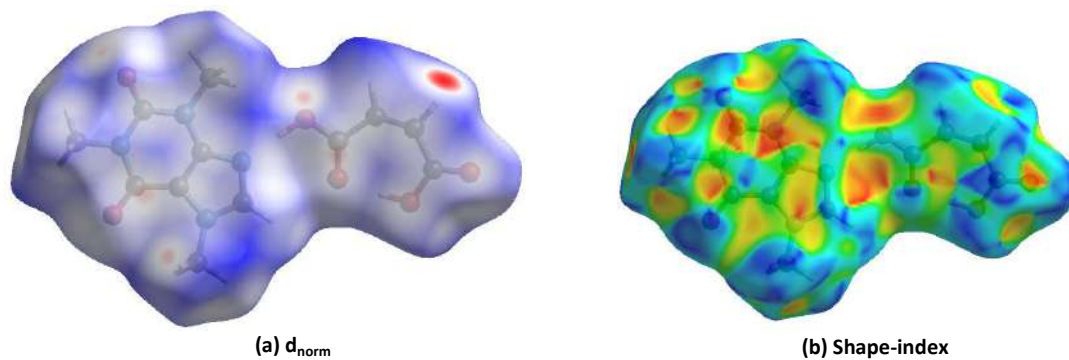


Fig. 4: Hirshfeld surfaces mapped with (a)  $d_{norm}$  and (b) shape-index

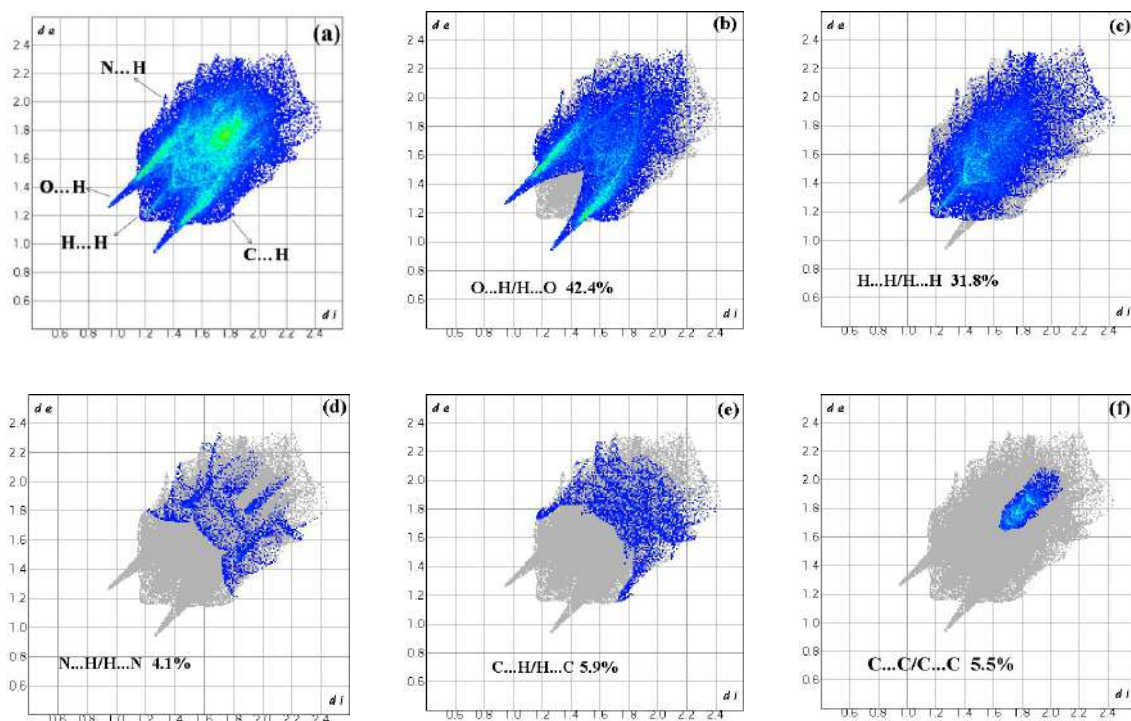


Fig. 5: The fingerprint plots: (a) For overall interactions, (b) For O...H/H...O interaction, (c) For H...H/H...H interaction (d) For N...H/H...N interaction, (e) For C...H/H...C interaction, and (e) For C...C/C...C interaction.

color region and possess a negative electrostatic potential, enabling them to function as nucleophiles. With negative potentials of  $-27.08$ ,  $-30.15$ , and  $-44.85$  kcal/mol, the atoms O3, O6, and O27 have been identified to be nucleophiles; O27 has the global minimum potential, indicating that it is the strong nucleophile. The hydrogen atoms H20, H22, H24, and H35 have positive electrostatic potentials of 26.03, 25.96, 37.63, and 25.65 kcal/mol, with H24 being the strongest electrophile among them, exhibiting the highest potential. The global minimum potential seen on O27 and maximum potential on H24 indicate that they are the probable sites of electrophilic and nucleophilic attack, respectively, which may form strong intermolecular hydrogen bonding for the crystal packing. This may lead to the conclusion that O...H interaction may be significant in the crystal packing of the caffeine-maleic acid cocrystal which was also revealed from the Hirshfeld surface analysis.

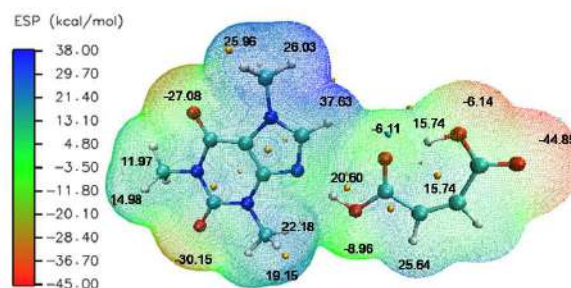


Fig.6. ESP mapped molecular vdW surface for the caffeine-maleic acid cocrystal.

### 3.6 Frontier molecular orbital and density of state

The frontier molecular orbital (FMO) model provides insight into the structure and reactivity of molecules by depicting the highest occupied molecular orbital (HOMO) and lowest unoccupied molecular orbital (LUMO) [39]. The energy gap

between HOMO and LUMO is used to predict molecular reactivity and kinetic stability. A molecule with a small energy gap is considered soft because it is more polarizable, which increases chemical reactivity [40]. The excitation of an electron from the valence band to the conduction band was revealed by a density of states. The HOMO–LUMO plot and DOS spectrum created with a full width at half maximum of 0.3 eV for the caffeine-maleic acid cocrystal are shown in Fig. 7. Caffeine-maleic acid cocrystals have an energy gap of 4.018 eV in gas and 3.670 eV in solvent water, indicating that it is more reactive and polarizable in solvent water than in gas. The HOMO–LUMO energy gap was found to be identical to the energy gap in the DOS spectrum. Rijal *et al.* calculated the energy gap between HOMO and LUMO for caffeine in the gaseous medium in solvent water at the B3LYP/6–311++G(d,p)

level of theory. They found that the energy gap in the gaseous medium is 5.04 eV and 5.08 eV in solvent water [7]. From this observation, we conclude that the caffeine-maleic acid cocrystal is more reactive, and more polarizable but kinetically less stable than the active pharmaceutical ingredient (API) caffeine. This leads to the conclusion that the physicochemical properties of the caffeine-maleic acid cocrystal were superior to those of API caffeine in terms of reactivity. In the Density of States (DOS) spectrum, a high-intensity peak indicates the presence of multiple states at various energy levels. The red and blue lines are attributed to the lowest unoccupied molecular orbital (LUMO) and the highest occupied molecular orbital (HOMO), respectively. The virtual orbital is associated with the acceptor orbital, while the occupied orbitals are considered donor orbitals.

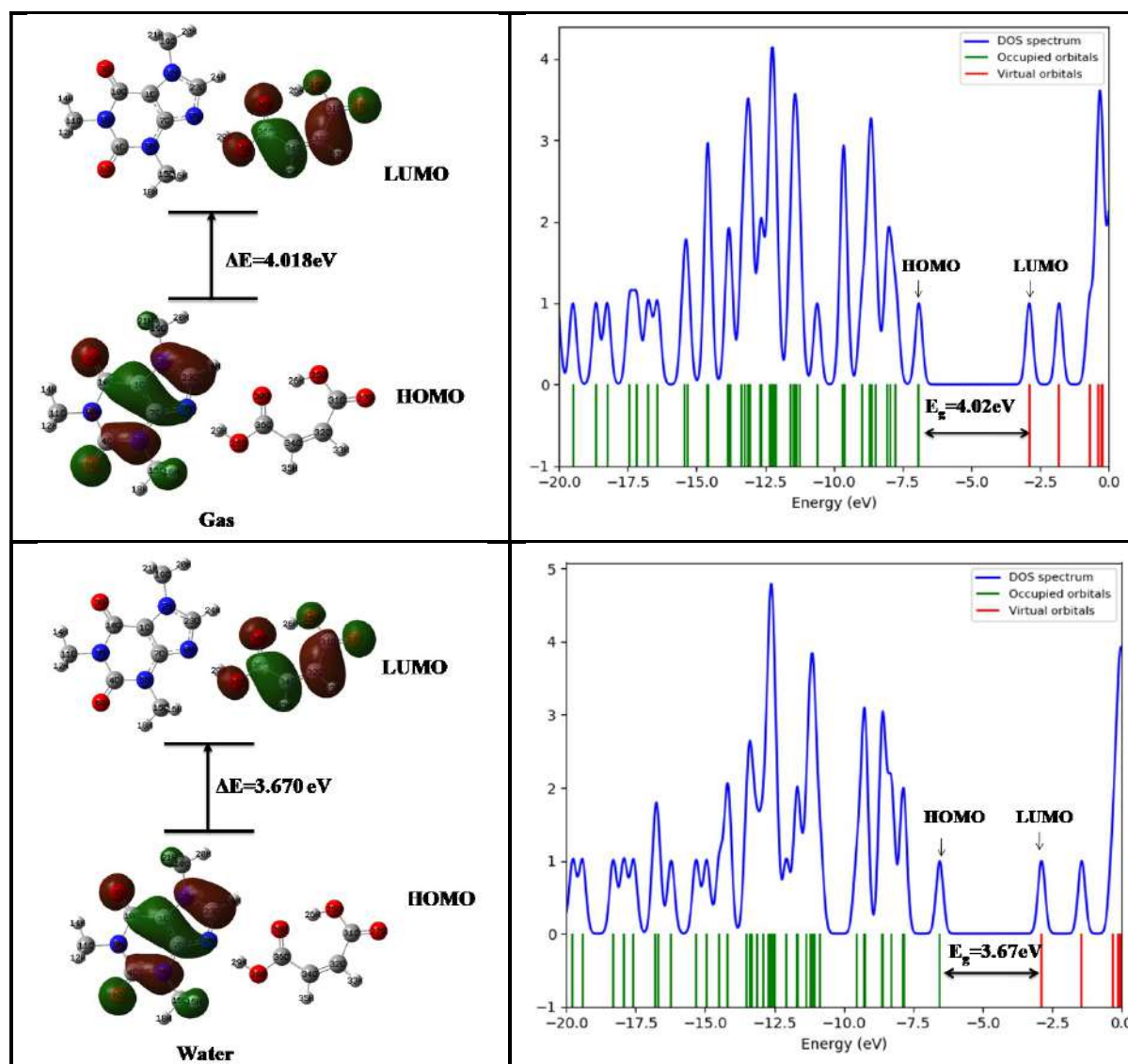


Fig. 7: HOMO–LUMO plots and DOS spectrum for the caffeine-maleic acid cocrystal in the gaseous medium and in solvent water.

### 3.7 Global reactivity descriptors

The global reactivity descriptors are chemical parameters used to predict chemical behavior, such as electrophilicity, nucleophilicity, reactivity, stability, and other reaction mechanism-related factors. The Koopman theorem suggests

that the ionization potential is the energy associated with HOMO, while the electron affinity is the energy associated with LUMO [41]. The following relations provide the reactivity descriptors electronegativity ( $\chi$ ), chemical potential ( $\mu$ ), global hardness ( $\eta$ ), softness ( $S$ ), and electrophilicity index ( $\omega$ )

in terms of ionization potential (I) and electron affinity (A) [42,43].

$$\text{Electronegativity } (\chi) = \frac{1}{2}(I + A)$$

$$\text{Chemical Potential } (\mu) = -\chi = -\frac{1}{2}(I + A)$$

$$\text{Global Hardness } (\eta) = \frac{1}{2}(I - A)$$

$$\text{Softness}(S) = \frac{1}{2\eta}$$

$$\text{Global Electrophilicity index } (\omega) = \frac{\mu^2}{2\eta}$$

The global reactivity descriptors for the caffeine-maleic acid cocrystal are displayed in Table 3. The electrophilicity index measures the tendency of a system to attract electrons from nucleophiles. The chemical potential and electrophilicity index

of the caffeine-maleic acid cocrystal are higher in solvent water as compared to that in gaseous medium, indicating that it is a good electrophile in solvent. The ionization potential in the gaseous medium is higher than in solvent water, indicating that this cocrystal is a good electron acceptor in a gaseous medium. The global hardness in gaseous medium is higher and softness is lower as compared to that in solvent water, which confirms that caffeine-maleic acid cocrystal is softer, polarizable, and reactive in solvent as compared to that in gaseous medium. The energy gap of the caffeine-maleic acid cocrystal in solvent water was found to be lower than that in gaseous medium; due to this, it is easier to donate an electron from HOMO to LUMO in solvent, and its chemical reactivity increases in water. The reason for the increase in reactivity in solvent water is that water facilitates the flow of charge.

**Table 3:** Global reactivity descriptors for the caffeine-maleic acid cocrystal.

Medium	I(eV)	A(eV)	(I-A)(eV)	$\chi$ (eV)	$\mu$ (eV)	$\eta$ (eV)	S(eV <sup>-1</sup> )	$\omega$ (eV)	$\Delta N_{max}$
Gaseous	6.9050	2.8870	4.0180	4.8960	-4.8960	2.0090	0.2489	5.9659	2.4370
Water	6.5440	2.8740	3.6700	4.7090	-4.7090	1.8350	0.2725	6.0421	2.5662

### 3.8 Natural bond orbital analysis

Natural bond orbital analysis is a reliable method for studying electron donor-acceptor charge transfer and conjugative interactions to gain insight into intra- and intermolecular bonding interactions [44]. The stabilization energy E(2) resulting from the interaction between electron donor and acceptor orbitals measures the intensity of that interaction. The donor and acceptor orbitals interact more strongly as the stabilizing energy increases [45]. In our study, NBO analysis was performed at the B3LYP/6-311++G(d,p) level of theory, and Table 4 shows the stabilization energy, as well as the donor and acceptor bonding interactions. The interactions LP(1)N2→π\*(N8-C23), LP(1)N5→π\*(C4-O6),

LP(1)N9→π\*(C4-O6), and LP(1)N9→π\*(O3-C10) within caffeine have stabilization energies of 67.01, 55.32, 55.72, and 52.28 kcal/mol, and the interactions LP(2)O25→π\*(O27-C31) and LP(2)O28→π\*(O30-C36) within maleic acid have stabilization energies of 51.21 and 59.69 kcal/mol. These interactions indicate that the caffeine-maleic acid cocrystal has stabilized, as evidenced by higher stabilization energy values. The intermolecular interaction for the hydrogen bonding between API caffeine and cofomer maleic acid is represented by the interaction LP(1)N8→π\*(O28-H29), which exhibits strong hydrogen bonding with a stabilization energy of 37.25 kcal/mol.

**Table 4.** NBO of the caffeine-maleic acid cocrystal by the analysis of second-order perturbation theory analysis of Fock matrix calculated at B3LYP/6-311++G(d,p) level of theory.

Donor NBO(i)	ED (i)/e	Acceptor NBO(j)	ED(j)/e	E(2) <sup>a</sup> kcal/mol	E(j)-E(i) <sup>b</sup>	Co F(i,j) <sup>c</sup> a.u
Within caffeine						
π(C1-C7)	1.730	π*(O3-C10)	0.351	28.00	0.30	0.083
π(C1-C7)	1.730	π*(N8-C23)	0.455	12.58	0.25	0.053
σ(N8-C23)	1.980	σ*(N5-C7)	0.037	7.09	1.29	0.086
π(N8-C23)	1.839	π*(C1-C7)	0.421	26.19	0.34	0.090
LP(1)N2	1.524	π*(N8-C23)	0.455	67.01	0.25	0.116
LP(1)N2	1.524	π*(C1-C7)	0.421	29.59	0.29	0.084
LP(2)O3	1.855	σ*(N9-C10)	0.097	28.53	0.64	0.122
LP(2)O3	1.855	σ*(C1-C10)	0.056	17.23	0.74	0.103
LP(1)N5	1.637	π*(C4-O6)	0.372	55.32	0.27	0.110
LP(1)N5	1.637	π*(C1-C7)	0.421	49.09	0.28	0.106
LP(2)O6	1.840	σ*(C4-N9)	0.084	26.10	0.64	0.118
LP(2)O6	1.840	σ*(C4-N5)	0.084	25.74	0.65	0.118
LP(1)N9	1.863	π*(C4-O6)	0.372	55.72	0.27	0.109
LP(1)N9	1.626	π*(O3-C10)	0.351	52.28	0.27	0.107
Caffeine to maleic acid						
LP(1)N8	1,863	σ*(O28-H29)		37.25	0.78	0.154

Within maleic acid						
$\pi(O27-C31)$	1.966	$\pi^*(C32-C34)$	0.049	6.91	0.39	0.046
$\sigma(C32-H33)$	1.972	$\sigma^*(C34-C36)$	0.058	6.99	0.93	0.072
$\pi(C32-C34)$	1.871	$\pi^*(O30-C36)$	0.309	19.00	0.28	0.068
$\pi(C32-C34)$	1.871	$\pi^*(O27-C31)$	0.246	12.04	0.32	0.057
LP(2)O27	1.860	$\sigma^*(C31-C32)$	0.074	18.49	0.63	0.098
LP(2)O25	1.788	$\pi^*(O27-C31)$	0.246	51.21	0.33	0.117
LP(2)O27	1.860	$\sigma^*(O25-C31)$	0.084	29.06	0.65	0.124
LP(1)O28	1.967	$\sigma^*(O30-C36)$	0.028	8.90	1.13	0.090
LP(2)O28	1.756	$\pi^*(O30-C36)$	0.309	59.69	0.31	0.124
LP(2)O30	1.845	$\sigma^*(O28-C36)$	0.067	25.37	0.72	0.123
LP(2)O30	1.845	$\sigma^*(O25-H26)$	0.067	25.21	0.74	0.125
LP(2)O30	1.845	$\sigma^*(C34-C36)$	0.058	11.41	0.73	0.083

<sup>a</sup>E(2) is the stabilization energy represented by hyper conjugative interaction .

<sup>b</sup>Energy difference between donor (i) and acceptor (j) NBO orbitals.

<sup>c</sup>F(i,j) is the element of the Fock matrix between NBO orbitals i and j.

#### 4. CONCLUSION

This study sheds light on the molecular interactions in the caffeine-maleic acid cocrystal. The intermolecular hydrogen bonds between caffeine and maleic acid (O28-H29...N8) created the cocrystal. The interaction energy in the formation of cocrystals was found to be -15.501 kcal/mol, which is in agreement with the interaction energy evaluated from the QTAIM analysis. The optimized structure parameters of the cocrystal were evaluated and compared to those of the crystal structure. Caffeine and maleic acid showed two intermolecular hydrogen bonds and one intra-molecular hydrogen bond, which were supported by QTAIM analysis and the RDG scatter and its isosurface. With a greater contribution of 42.4% to the Hirshfeld surface, the intermolecular interaction caused by O...H demonstrates its critical role in the crystal packing of the cocrystal of caffeine and maleic acid. The global minimum electrostatic potential of -44.85 kcal/mol attributed to O27 and the highest positive potential of 37.63 kcal/mol attributed to H24 suggested the sites of intermolecular hydrogen bonding from ESP analysis in the packing of the crystal, which also support the fingerprint plot of Hirshfeld surface analysis. The energy gap of the caffeine-maleic acid cocrystal was found to be less compared to that of API caffeine, indicating that the cocrystal is more reactive and more polarizable. Compared to a gaseous medium, the caffeine-maleic acid cocrystal was found to be more reactive in solvent water. According to the natural bond orbital analysis, the interaction LP(1)N8→ $\pi^*(O28-H29)$  is responsible for the intermolecular hydrogen bonding between API caffeine and coformer maleic acid, with a stabilization energy of 37.25 kcal/mol indicating a strong interaction.

#### AUTHOR CONTRIBUTIONS

T.R. Paneru: Conceptualization of research activity, investigation, data analysis, writing original draft; B. Bhandari: Reviewing, analysis of result, and proofreading.

#### ETHICAL ISSUE

The authors declare no ethical issues.

#### CONFLICT OF INTEREST

There are no conflicts to declare.

#### ACKNOWLEDGMENTS

T.R. Paneru acknowledges University Grants Commission (UGC), Nepal, for providing partial research support through the Research Fellowship (UGC Award No. PhD-079/80-ST-18), and he also acknowledges Far Western University, Mahendranagar, Nepal.

#### REFERENCES

- [1] S.N. Wong, Y.C.S. Chen, B. Xuan, C.C. Sun, S.F. Chow, Cocrystal engineering of pharmaceutical solids: therapeutic potential and challenges, *Cryst Eng Comm* 23 (2021) 7005–7038. <https://doi.org/10.1039/D1CE00825K>
- [2] M. Guo, X. Sun, J. Chen, T. Cai, Pharmaceutical cocrystals: A review of preparations, physicochemical properties and applications, *Acta Pharmaceutica Sinica B* 11 (2021) 2537–2564. <https://doi.org/10.1016/j.apsb.2021.03.030>
- [3] T.R. Paneru, M.K. Chaudhary, B.D. Joshi, P. Tandon, Cocrystal screening of benzimidazole based on electronic transition, molecular reactivity, hydrogen bonding, and stability, *J Mol Model* 30 (2024) 378. <https://doi.org/10.1007/s00894-024-06146-1>
- [4] T.R. Shattock, K.K. Arora, P. Vishweshwar, M.J. Zaworotko, Hierarchy of supramolecular synthons: persistent carboxylic acid...pyridine hydrogen bonds in cocrystals that also contain a hydroxyl moiety, *Cryst. Growth Des.* 8 (2008) 4533–4545. <https://doi.org/10.1021/cg800565a>
- [5] S. Aitipamula, R.B.H. Tan, 1. Pharmaceutical cocrystals: crystal engineering and applications, in: E. Tiekink, J. Zukerman (Eds.), *Multi-Component Crystals*, De Gruyter, 2017: pp. 1–31. <https://doi.org/10.1515/9783110464955-001>
- [6] J. Evans, J.R. Richards, A.S. Battisti, Caffeine, in: *StatPearls*, StatPearls Publishing, Treasure Island (FL), 2024. <http://www.ncbi.nlm.nih.gov/books/NBK519490>.
- [7] R. Rijal, M. Sah, H.P. Lamichhane, H.S. Mallik, Quantum chemical calculations of nicotine and caffeine molecule in gas phase and solvent using DFT methods, *Heliyon* 8 (2022) e12494. <https://doi.org/10.1016/j.heliyon.2022.e12494>

- [8] B.F. Harland, Caffeine and nutrition, *Nutrition* 16 (2000) 522–526. [https://doi.org/10.1016/S0899-9007\(00\)00369-5](https://doi.org/10.1016/S0899-9007(00)00369-5)
- [9] A.V. Trask, W.D.S. Motherwell, W. Jones, Pharmaceutical cocrystallization: Engineering a remedy for caffeine hydration, *Cryst Growth Des* 5 (2005) 1013–1021. <https://doi.org/10.1021/cg0496540>
- [10] K. Guo, G. Sadiq, C. Seaton, R. Davey, Q. Yin, Cocrystallization in the Caffeine/Maleic Acid System: Lessons from Phase Equilibria, *Cryst Growth Des* 10 (2010) 268–273. <https://doi.org/10.1021/cg900885n>
- [11] T. Leysens, G. Springuel, R. Montis, N. Candoni, S. Veessler, Importance of solvent selection for stoichiometrically diverse cocrystal systems: Caffeine/maleic Acid 1:1 and 2:1 cocrystals, *Cryst Growth Des* 12 (2012) 1520–1530. <https://doi.org/10.1021/cg201581z>
- [12] S. Aher, R. Dhumal, K. Mahadik, A. Paradkar, P. York, Ultrasound assisted cocrystallization from solution (USSC) containing a non-congruently soluble cocrystal component pair: Caffeine/maleic acid, *Eur J Pharm Sci* 41 (2010) 597–602. <https://doi.org/10.1016/j.ejps.2010.08.012>
- [13] P. Hohenberg, W. Kohn, Inhomogeneous Electron Gas, *Phys Rev* 136 (1964) B864–B871. <https://doi.org/10.1103/PhysRev.136.B864>
- [14] M.J. Frisch, G.W. Trucks, H.B. Schlegel, G.E. Scuseria, M.A. Robb, J.R. Cheeseman, G. Scalmani, V. Barone, B. Mennucci, G.A. Petersson, H. Nakatsuji, M. Caricato, X. Li, H.P. Hratchian, A.F. Izmaylov, J. Bloino, G. Zheng, J.L. Sonnenberg, M. Hada, M. Ehara, K. Toyota, R. Fukuda, J. Hasegawa, M. Ishida, T. Nakajima, Y. Honda, O. Kitao, H. Nakai, T. Vreven, J.A. Montgomery, J.E. Peralta, F. Ogliaro, M. Bearpark, J.J. Heyd, E. Brothers, K.N. Kudin, V.N. Staroverov, R. Kobayashi, J. Normand, K. Raghavachari, A. Rendell, J.C. Burant, S.S. Iyengar, J. Tomasi, M. Cossi, N. Rega, J.M. Millam, M. Klene, J.E. Knox, J.B. Cross, V. Bakken, C. Adamo, J. Jaramillo, R. Gomperts, R.E. Stratmann, O. Yazyev, A.J. Austin, R. Cammi, C. Pomelli, J.W. Ochterski, R.L. Martin, K. Morokuma, V.G. Zakrzewski, G.A. Voth, P. Salvador, J.J. Dannenberg, S. Dapprich, A.D. Daniels, Ö. Farkas, J.B. Foresman, J.V. Ortiz, J. Cioslowski, D.J. Fox, Gaussian 9 Revision, Gaussian, Inc. Wallingford (2009).
- [15] A.D. Becke, Density-functional thermochemistry. III. The role of exact exchange, *J Chem Phys* 98 (1993) 5648–5652. <https://doi.org/10.1063/1.464913>
- [16] T.H. Dunning, Gaussian basis sets for use in correlated molecular calculations. I. The atoms boron through neon and hydrogen, *J Chem Phys* 90 (1989) 1007–1023. <https://doi.org/10.1063/1.456153>
- [17] R. Dennington, T.A. Keith, Millam, M. John, GaussView 05 Semichem Inc., Shawnee Mission, KS (2009).
- [18] T.A. Keith, AIMALL version (19.10.12) TK Gristmill Software, Overland Park KS. USA, (2019). <http://aim@tkgristmill.com/>.
- [19] M. Turner, J. McKinnon, S. Wolff, D. Grimwood, P. Spackman, D. Jayatilaka, M. Spackman, *CrystalExplorer17*, (2017).
- [20] T. Lu, F. Chen, Multiwfn: A multifunctional wavefunction analyzer, *J Comput Chem* 33 (2012) 580–592. <https://doi.org/10.1002/jcc.22885>
- [21] W. Humphrey, A. Dalke, K. Schulten, VMD: Visual molecular dynamics, *J Mol Graph* 14 (1996) 33–38. [https://doi.org/10.1016/0263-7855\(96\)00018-5](https://doi.org/10.1016/0263-7855(96)00018-5)
- [22] N.M. O'boyle, A.L. Tenderholt, K.M. Langner, cclib: A library for package-independent computational chemistry algorithms, *J Comput Chem* 29 (2008) 839–845. <https://doi.org/10.1002/jcc.20823>
- [23] E.D. Glendening, A.E. Reed, J.E. Carpenter, F. Weinhold, NBO 3.0 Program manual, Theor Chem Inst, University of Wisconsin, Madison, WI (1996).
- [24] A.V. Trask, W.D.S. Motherwell, W. Jones, CCDC 272622: Experimental Crystal Structure Determination, (2005). <https://doi.org/10.5517/CC94P8C>
- [25] R.F.W. Bader, S.G. Anderson, A.J. Duke, Quantum topology of molecular charge distributions. 1, *J Am Chem Soc* 101 (1979) 1389–1395. <https://doi.org/10.1021/ja00500a006>
- [26] S.J. Grabowski, Non-covalent interactions – QTAIM and NBO analysis, *J Mol Model* 19 (2013) 4713–4721. <https://doi.org/10.1007/s00894-012-1463-7>
- [27] U. Koch, P.L.A. Popelier, Characterization of C-H-O hydrogen bonds on the basis of the charge density, *J Phys Chem* 99 (1995) 9747–9754. <https://doi.org/10.1021/j100024a016>
- [28] I. Rozas, I. Alkorta, J. Elguero, Behavior of ylides containing N, O, and C atoms as hydrogen bond acceptors, *J Am Chem Soc* 122 (2000) 11154–11161. <https://doi.org/10.1021/ja0017864>
- [29] E.R. Johnson, S. Keinan, P. Mori-Sánchez, J. Contreras-García, A.J. Cohen, W. Yang, Revealing Noncovalent Interactions, *J Am Chem Soc* 132 (2010) 6498–6506. <https://doi.org/10.1021/ja100936w>
- [30] G. Saleh, C. Gatti, L. Lo Presti, Non-covalent interaction via the reduced density gradient: Independent atom model vs experimental multipolar electron densities, *Comput Theor Chem* 998 (2012) 148–163. <https://doi.org/10.1016/j.comptc.2012.07.014>
- [31] T.R. Paneru, M.K. Chaudhary, P. Tandon, T. Chaudhary, B.D. Joshi, Theoretical study on molecular stability, reactivity, and drug potential of cirsilineol from DFT and molecular docking methods, *Chem Phys Impact* 8 (2024) 100641. <https://doi.org/10.1016/j.chphi.2024.100641>
- [32] F.L. Hirshfeld, Bonded-atom fragments for describing molecular charge densities, *Theor Chim. Acta* 44 (1977) 129–138. <https://doi.org/10.1007/BF00549096>
- [33] P.R. Spackman, M.J. Turner, J.J. McKinnon, S.K. Wolff, D.J. Grimwood, D. Jayatilaka, M.A. Spackman, *CrystalExplorer*: a program for Hirshfeld surface analysis, visualization and quantitative analysis of molecular crystals, *J Appl Crystallogr* 54 (2021) 1006–1011. <https://doi.org/10.1107/S1600576721002910>
- [34] A. Khurshid, A. Saeed, T. Hökelek, U. Taslim, M. Irfan, S.U. Khan, A. Iqbal, H.R. El-Seedi, Experimental and Hirshfeld surface investigations for unexpected aminophenazone cocrystal formation under thiourea reaction conditions via possible enamine assisted rearrangement, *Crystals* 12 (2022) 608. <https://doi.org/10.3390/cryst12050608>
- [35] K.L. Jyothi, R. Gautam, D. Swain, T.N. Guru Row, N.K. Lokanath, Cocrystals of gallic acid with urea and propionamide: Supramolecular Structures, Hirshfeld surface analysis, and DFT studies, *Cryst Res Tech* 54 (2019) 1900016. <https://doi.org/10.1002/crat.201900016>
- [36] P.K. Weiner, R. Langridge, J.M. Blaney, R. Schaefer, P.A. Kollman, Electrostatic potential molecular surfaces., *Proc Natl Acad Sci U.S.A.* 79 (1982) 3754–3758. <https://doi.org/10.1073/pnas.79.12.3754>

- [37] B.D. Joshi, Chemical Reactivity, Dipole Moment and First Hyperpolarizability of Aristolochic Acid I, *J Inst Sci Tech* 21 (2016) 1–9. <https://doi.org/10.3126/iist.v21i1.16030>
- [38] F.R. B., J.C. Prasana, S. Muthu, C.S. Abraham, Molecular docking studies, charge transfer excitation and wave function analyses (ESP, ELF, LOL) on valacyclovir: A potential antiviral drug, *Comput Bio Chem* 78 (2019) 9–17. <https://doi.org/10.1016/j.compbiolchem.2018.11.014>
- [39] J. Yu, N.Q. Su, W. Yang, Describing chemical reactivity with frontier molecular orbitals, *JACS Au* 2 (2022) 1383–1394. <https://doi.org/10.1021/jacsau.2c00085>
- [40] H.A. Hussein, G.F. Fadhil, Theoretical investigation of *para* amino-dichloro chalcone isomers. part II: A DFT structure–stability study of the FMO and NLO properties, *ACS Omega* 8 (2023) 4937–4953. <https://doi.org/10.1021/acsomega.2c07148>
- [41] T. Koopmans, Über die Zuordnung von Wellenfunktionen und Eigenwerten zu den einzelnen Elektronen eines Atoms, *Physica* 1 (1934) 104–113. [https://doi.org/10.1016/S0031-8914\(34\)90011-2](https://doi.org/10.1016/S0031-8914(34)90011-2)
- [42] R.G. Parr, R.G. Pearson, Absolute hardness: companion parameter to absolute electronegativity, *J Am Chem Soc* 105 (1983) 7512–7516. <https://doi.org/10.1021/ja00364a005>
- [43] R.G. Parr, L.V. Szentpály, S. Liu, Electrophilicity Index, *J Am Chem Soc* 121 (1999) 1922–1924. <https://doi.org/10.1021/ja983494x>
- [44] S. Sebastian, N. Sundaraganesan, The spectroscopic (FT-IR, FT-IR gas phase, FT-Raman and UV) and NBO analysis of 4-Hydroxypiperidine by density functional method, *Spectrochim Acta A Mol Biomol Spectrosc* 75 (2010) 941–952. <https://doi.org/10.1016/j.saa.2009.11.030>
- [45] F. Weinhold, C.R. Landis, Valency and Bonding: A Natural Bond Orbital Donor-Acceptor Perspective, Cambridge University Press, 2005.